Thermodynamic Analysis of the Fe–Cr–B Ternary System

Kenta Yamada[2], Hiroshi Ohtani[1], Mitsuhiro Hasebe[1]

[1]*Department of Materials Science and Engineering, Kyushu Institute of Technology, Kitakyushu 804-8550, Japan*
[2]*Graduate School, Kyushu Institute of Technology, Kitakyushu 804-8550, Japan*

(Received January 5,2009;final form January 13,2009)

ABSTRACT

A thermodynamic analysis of the Fe–Cr–B ternary system was carried out to clarify the complex phase equilibria between several types of borides and solution phases. To satisfy the lack of experimental information on thermodynamic properties for this ternary system, a first-principles method was applied to evaluate the enthalpies of formation of binary Cr-boride phases. The calculated enthalpy of formation of CrB_2 agreed well with the experimental value. However, the first-principles calculations suggested that the CrB phase is more stable in the ground state than previously thought. Variations of the formation enthalpies of Fe_2B (*I4/mcm*) and CrB (*Cmcm*) with dissolving Cr and Fe were also evaluated for superstructures constructed by modifying the stack of atoms along a given direction of the parent lattice structures. The thermodynamic parameters of the Fe–Cr–B ternary system were optimized with the CALPHAD technique using these calculated thermodynamic properties along with available experimental information on phase equilibria and some thermodynamic data. We found that the evaluated parameters reasonably reproduced the experimental data on the isothermal sections, the pseudo-binary section, and the liquidus projection in the Fe-rich region.

Keywords: Phase diagram, thermodynamic analysis, CALPHAD, first-principles calculations, borides.

1. INTRODUCTION

It is well known that addition of small amounts of boron (B) to steels enhances mechanical properties such as microhardness or tensile strength. This is partly due to segregation of B at grain boundaries. For instance, segregated B at the austenite grain boundaries is thought to improve the hardenability of steels through control of the ferritic transformation. Boron also acts to form B-containing precipitates, such as $(Fe,Cr)_{23}(B,C)_6$, which increase the creep rapture life of stainless steels at high temperatures. On the other hand, B plays an essential role in producing Fe-based bulk amorphous alloys with a wider supercooled liquid region and desirable soft magnetic properties. Despite these important roles in industrial materials, the behavior of B in ferrous alloys, in particular its role in phase equilibria in stainless steels, is still unclear. This is partly to be attributed to the experimental difficulty of characterizing an element with a rather low atomic number.

The Fe–Cr–B ternary phase diagram is composed of several boride phases, namely Fe_2B, FeB, Cr_2B, Cr_5B_3, CrB, Cr_3B_4, CrB_2, and CrB_4, and these borides complicate the phase equilibria in this ternary system. Isothermal section diagrams, as well as pseudobinary FeB–CrB sections, were experimentally studied for the system; however, thermodynamic analysis is required for understanding the role of B in steels. The purpose of the present study was to clarify the phase equilibria of the Fe–Cr–B ternary system over the entire composition

and temperature ranges, by evaluating the thermodynamic properties of various borides using a first-principles energetic calculation method and estimating the unknown phase equilibria using these theoretical values, as well as any available experimental information.

2. COMPUTATIONAL PROCEDURE

2.1 Evaluation of enthalpy of formation for borides at zero temperature using first-principles calculations

The enthalpy of formation of the boride phases was calculated using the full potential linearized augmented plane wave (FLAPW) method. The FLAPW method, as embodied in the WIEN2k software package /1/, is one of the most accurate schemes for electronic calculations and allows precise calculations of the total energies in solids. Therefore, this method is most appropriate for evaluation of a relative thermodynamic property such as the formation enthalpy. The exchange-correlation functional was described by the generalized gradient approximation (GGA) of the Perdew–Burke–Ernzerhof 96 form /2/. The plane-wave cutoff energy was set at 270 eV throughout the calculation.

2.2 Thermodynamic modeling of the solution phases

A description of the Gibbs energy for each phase appearing in the Fe–Cr–B ternary system is presented in this section.

2.2.1 Liquid (L), bcc (α and δ), and fcc (γ) solution phases

The regular solution approximation was applied to the liquid phase, as well as the α, δ and γ solid solutions. Solid solutions of B in both bcc and fcc Fe are known to exhibit both substitutional and interstitial characters, as shown by several thermodynamic studies. Recently our group found that at least in the ground state, the solid solution model in which B atoms substitute for Fe atoms was more probable than the one in which dissolved B atoms occupied octahedral interstitial sites /3/. Based on this knowledge, we applied the regular solution approximation to the solid solutions as well as to the liquid phase in the Fe–Cr–B system.

The molar Gibbs energy, G_m^{ϕ}, was described as:

$$G_m^{\phi} = x_B\,{}^{o}G_B^{\phi} + x_{Cr}\,{}^{o}G_{Cr}^{\phi} + x_{Fe}\,{}^{o}G_{Fe}^{\phi} + RT(x_B \ln x_B + x_{Cr} \ln x_{Cr} + x_{Fe} \ln x_{Fe}) + x_B x_{Cr} L_{B,Cr}^{\phi} + x_B x_{Cr} \bar{L}_{B,Cr}^{\phi} + x_{Cr} x_{Fe} L_{Cr,Fe}^{\phi} + x_B x_{Cr} x_{Fe} L_{B,Cr,Fe}^{\phi}, \quad (1)$$

where ${}^{o}G_i^{\phi}$ denotes the molar Gibbs energy of element i in the ϕ state. This quantity is called "the lattice stability parameter" and is described by the following formula:

$${}^{o}G_i^{\phi} - {}^{o}H_i^{ref} = A + BT + CT\ln T + DT^2 + ET^3 + FT^7 + IT^{-1} + JT^{-9}, \quad (2)$$

where ${}^{o}H_i^{ref}$ denotes the molar enthalpy of the pure element i in its stable state at T = 298 K. The parameter $L_{i,j}^{\phi}$ denotes the interaction energy between i and j in the ϕ phase and has a compositional dependency following the Redlich–Kister polynomial as:

$$L_{i,j}^{\phi} = {}^{0}L_{i,j}^{\phi} + {}^{1}\bar{L}_{i,j}^{\phi}(x_i - x_j) + {}^{2}L_{i,j}^{\phi}(x_i - x_j)^2, \quad (3)$$

where the temperature dependency was introduced as ${}^{n}L_{i,j}^{\phi} = a + bT$.

The term $L_{B,Cr,Fe}^{\phi}$ is the ternary interaction parameter between the elements B, Cr, and Fe. The dependence of the interaction parameters on composition is expressed as follows:

$$L_{B,Cr,Fe}^{\phi} = x_B\,{}^{0}L_{B,Cr,Fe}^{\phi} + x_{Cr}\,{}^{1}L_{B,Cr,Fe}^{\phi} + x_{Fe}\,{}^{2}L_{B,Cr,Fe}^{\phi} \quad (4)$$

2.2.2 The FeB, Fe_2B, CrB, Cr_2B, and Cr_5B_3 phases

The binary compounds FeB, Fe_2B, CrB, Cr_2B, and Cr_5B_3 dissolve the third element to some extent. Therefore, the two-sublattice model denoted by $\left(Cr_{y_{Cr}^{(1)}}Fe_{y_{Fe}^{(1)}}\right)_{u_1}\left(B_{y_B^{(2)}=1}\right)_{u_2}$ was applied to these phases, where u_1 and u_2 are the numbers of the sites of the sublattices in parentheses. The Gibbs energy per mole of formula unit of these phases is given by:

$$G_m^{\phi} = y_{Cr}^{(1)}\,{}^{\circ}G_{Cr:B}^{\phi} + y_{Fe}^{(1)}\,{}^{\circ}G_{Fe:B}^{\phi} + u_1 RT(y_{Cr}^{(1)}\ln y_{Cr}^{(1)} + y_{Fe}^{(1)}\ln y_{Fe}^{(1)}) + y_{Cr}^{(1)}y_{Fe}^{(1)}L_{Cr,Fe:B}^{\phi} \quad (5)$$

The quantity $y_i^{(j)}$ is the site fraction of element i in the respective sublattice, which is designated by (j). The value of ${}^{\circ}G_{i:B}^{\phi}$ denotes the Gibbs energy of the compound, $i_{u_1}B_{u_2}$. The parameter $L_{Cr.Fe:B}^{\phi}$ is the interaction parameter between unlike atoms on the first sublattice.

2.2.3. The σ phase

The Gibbs energy of the σ phase with some homogeneity range was described by the three-sublattice model, in which 30 atomic sites of the unit cell were divided into three sublattices, $\left(Fe_{y_{Fe}^{(1)}=1}\right)_8\left(Cr_{y_{Cr}^{(2)}=1}\right)_4\left(Cr_{y_{Cr}^{(3)}}Fe_{y_{Fe}^{(3)}}\right)_{18}$. The Gibbs energy of this phase was described by the following equation:

$$G_m^{\sigma} = y_{Cr}^{(3)}\,{}^{\circ}G_{Fe:Cr:Cr}^{\sigma} + y_{Fe}^{(3)}\,{}^{\circ}G_{Fe:Cr:Fe}^{\sigma} + \frac{18}{30}RT(y_{Cr}^{(3)}\ln y_{Cr}^{(3)} + y_{Fe}^{(3)}\ln y_{Fe}^{(3)}) \quad (6)$$

The interaction parameters having null values after the optimization process were excluded from the above description.

2.2.4 The stoichiometric compounds

The Cr–B binary compound phases with a zero homogeneity range (i.e., Cr_3B_4, CrB_2, CrB_4) were treated as being stoichiometric compounds. The Gibbs energy of the Cr_mB_n phase was expressed using the following equation, adopting the stable structure of the elements as the thermodynamic standard state:

$$G_{Cr:B}^{Cr_mB_n} - m\,{}^{\circ}G_{Cr}^{bcc-Cr} - n\,{}^{\circ}G_B^{rhombohedral-B} = a + bT + cT\ln T + dT^2 \quad (7)$$

2.2.5 Contribution of magnetic transitions to the Gibbs energy

The contribution caused by any magnetic ordering to the Gibbs free energy was added to the nonmagnetic part of the free energy, as follows:

$$G^{\phi} = G_m^{\phi} + G_{mag}^{\phi}. \quad (8)$$

The magnetic Gibbs energy, G_{mag}^{ϕ}, is given by the following expression /4,5/:

$$G_{mag}^{\phi} = RT\cdot f(\tau)\ln(\beta+1), \quad (9)$$

where

$$f(\tau) = 1 - \frac{1}{A}\left\{\frac{79\tau^{-1}}{140p} + \frac{474}{497}\left(\frac{1}{p}-1\right)\left(\frac{\tau^3}{6} + \frac{\tau^9}{135} + \frac{\tau^{15}}{600}\right)\right\}, \quad \text{for } \tau < 1, \quad (10)$$

and

$$f(\tau) = -\frac{1}{A}\left(\frac{\tau^{-5}}{10} + \frac{\tau^{-15}}{315} + \frac{\tau^{-25}}{1500}\right), \quad \text{for } \tau \geq 1, \quad (11),$$

and

$$A = \frac{518}{1125} + \frac{11692}{15975}\left(\frac{1}{p}-1\right). \quad (12)$$

The variable τ is defined as T / T_C, where T_C is the Curie temperature, and β is the mean atomic moment expressed in Bohr magnetons, μ_B. The parameter p depends on the crystal structure, and its value is 0.4 and 0.28 for the bcc and fcc phases, respectively.

3. THERMODYNAMIC ANALYSIS AND CALCULATION OF PHASE DIAGRAMS

A brief outline of the thermodynamic analysis and the calculated results is presented in this section. Most of the descriptions of the lattice stability parameters for each pure element were obtained from the Scientific Group Thermodata Europe (SGTE) data set /6/ and are shown in Table 1.

Table 1
Lattice stability parameters for Fe, Cr and B.

Element	Phase		Lattice stability parameters (J/mol)	Temperature range (K)	Reference
B	L	${}^{\circ}G_B^L - {}^{\circ}H_B^{(\beta B)}$	$= +40723.275 + 86.843839\,T - 15.6641\,T\ln T - 0.006864515\,T^2 + 6.18878\times10^{-7}T^3 + 370843\,T^{-1}$	$298.15 < T < 500$	[6]
			$= +41119.703 + 82.101722\,T - 14.9827763\,T\ln T - 0.007095669\,T^2 + 5.07347\times10^{-7}T^3 + 335484\,T^{-1}$	$500 < T < 2348$	
			$= +28842.012 + 200.94731\,T - 31.4\,T\ln T$	$2348 < T < 6000$	
	α	${}^{\circ}G_B^{\alpha} - {}^{\circ}H_B^{(\beta B)}$	$= +35778.716 + 94.894864\,T - 15.6641\,T\ln T - 0.006864515\,T^2 + 6.18878\times10^{-7}T^3 + 370843\,T^{-1}$	$298.15 < T < 1100$	
			$= +26864.526 + 172.584744\,T - 26.6047\,T\ln T - 7.9809\times10^{-4}T^2 - 2.556\times10^{-8}T^3 + 1748270\,T^{-1}$	$1100 < T < 2348$	
			$= +6846.418 + 219.119244\,T - 31.5957527\,T\ln T - 0.00159488\,T^2 + 1.34719\times10^{-7}T^3 + 11205883\,T^{-1}$	$2348 < T < 3000$	
	(βB)	${}^{\circ}G_B^{(\beta B)} - {}^{\circ}H_B^{(\beta B)}$	$= -7735.284 + 107.11864\,T - 15.6641\,T\ln T - 0.006864515\,T^2 + 6.18878\times10^{-7}T^3 + 370843\,T^{-1}$	$298.15 < T < 1100$	
			$= -16649.474 + 184.801744\,T - 26.6047\,T\ln T - 7.9809\times10^{-4}T^2 - 2.556\times10^{-8}T^3 + 1748270\,T^{-1}$	$1100 < T < 2348$	
			$= -36667.582 + 231.336244\,T - 31.5957527\,T\ln T - 0.00159488\,T^2 + 1.34719\times10^{-7}T^3 + 11205883\,T^{-1}$	$2348 < T < 3000$	
			$= -21530.653 + 222.396264\,T - 31.4\,T\ln T$	$3000 < T < 6000$	
	γ	${}^{\circ}G_B^{\gamma} - {}^{\circ}H_B^{(\beta B)}$	$= +35778.716 + 94.894864\,T - 15.6641\,T\ln T - 0.006864515\,T^2 + 6.18878\times10^{-7}T^3 + 370843\,T^{-1}$	$298.15 < T < 1100$	
			$= +26864.526 + 172.584744\,T - 26.6047\,T\ln T - 7.9809\times10^{-4}T^2 - 2.556\times10^{-8}T^3 + 1748270\,T^{-1}$	$1100 < T < 2348$	
			$= +6846.418 + 219.119244\,T - 31.5957527\,T\ln T - 0.00159488\,T^2 + 1.34719\times10^{-7}T^3 + 11205883\,T^{-1}$	$2348 < T < 3000$	
			$= +21983.347 + 210.179264\,T - 31.4\,T\ln T$	$3000 < T < 6000$	

Cr	L	${}^{\circ}G^{L}_{Cr} - {}^{\circ}G^{\alpha}_{Cr}$	$= +24339.955 - 11.420225\,T + 2.37615 \times 10^{-21} T^{7}$	298.15 < T < 2180
		${}^{\circ}G^{L}_{Cr} - {}^{\circ}H^{\alpha}_{Cr}$	$= -16459.984 + 335.616316\,T - 50\,T \ln T$	2180 < T < 6000
	α	${}^{\circ}G^{\alpha}_{Cr} - {}^{\circ}H^{\alpha}_{Cr}$	$= -8856.94 + 157.48\,T - 26.908\,T \ln T - 0.0189435\,T^{2} - 1.47721 \times 10^{-6} T^{3} + 139250\,T^{-1}$	298.15 < T < 2180
			$= -34869.344 + 344.18\,T - 50\,T \ln T - 2.88526 \times 10^{32} T^{-9}$	2180 < T < 6000
		$Tc^{\gamma}_{Cr} = -311.5$, $\beta^{\gamma}_{Cr} = -0.008$		298.15 < T < 6000
	γ	${}^{\circ}G^{\gamma}_{Cr} - {}^{\circ}G^{\alpha}_{Cr}$	$= +7284 + 0.163\,T$	298.15 < T < 6000
		$Tc^{\gamma}_{Cr} = -1109$, $\beta^{\gamma}_{Cr} = -246$		
Fe	L	${}^{\circ}G^{L}_{Fe} - {}^{\circ}H^{\alpha}_{Fe}$	$= +12040.17 - 6.55843\,T - 3.67516 \times 10^{-21} T^{7}$	298.15 < T < 1811
			$= -10838.83 + 291.302\,T - 46\,T \ln T$	1811 < T < 6000
	α	${}^{\circ}G^{\alpha}_{Fe} - {}^{\circ}H^{\gamma}_{Fe}$	$= +1225.7 + 124.134\,T - 23.5143\,T \ln T - 0.00439752\,T^{2} - 5.8927 \times 10^{-8} T^{3} + 77359\,T^{-1}$	298.15 < T < 1811
			$= -25383.581 + 299.31255\,T - 46\,T \ln T + 2.29603 \times 10^{31} T^{-9}$	1811 < T < 6000
		$Tc^{\gamma}_{Fe} = 1043$, $\beta^{\gamma}_{Fe} = 2.22$		298.15 < T < 6000
	γ	${}^{\circ}G^{\gamma}_{Fe} - {}^{\circ}H^{\alpha}_{Fe}$	$= -1462.4 + 8.282\,T - 1.15\,T \ln T + 6.4 \times 10^{-4} T^{2}$	298.15 < T < 1811
			$= -1713.815 + 0.94001\,T + 4.9251 \times 10^{30} T^{-9}$	1811 < T < 6000
		$Tc^{\gamma}_{Fe} = -201$, $\beta^{\gamma}_{Fe} = -2.1$		298.15 < T < 6000

[6]

[6]

Table 2

The calculated thermodynamic parameters of the borides.

System	Phase		Space group	Composition, (mol%B)	Enthalpy of formation, (kJ/mol)		
					First principles	Experimental	assessed
Cr–B	Cr_2B		*Fddd*	33.333	–38.5	–	–30.8[23]
	Cr_5B_3		*I4/mcm*	37.5	–39.7	–	–34.2[23]
	CrB		*Cmcm*	50	–56.5	–	–37.8[23]
	Cr_3B_4		*Immm*	57.143	–46.7	–	–42.9[23]
	CrB_2		*P6/mmm*	66.667	–33.3	–31.3 to –39.7[19]	–39.7[23]
	CrB_4		*Immm*	80	–23.6	–	–
Fe–Cr–B	(Fe,Cr)B	FeB	*Cmcm*	50	–35.1	–35.6 ± 6.3[31], –46.5[32], –32.3 ± 2.2[33]	–
		Fe_3CrB_4	*Cmcm*	50	–33.4	–	–
		$FeCrB_2$	$P2_1/m$	50	–42.6	–	–
		CrB	*Cmcm*	50	–53.2	–	–
	$(Fe,Cr)_2B$	Fe_2B	*I4/mcm*	33.333	–30.6	–22.3 ± 7.0[31], –33.8[32], –22.6 ± 2.7[33]	–
		Fe_7CrB_4	*Amm2*	33.333	–23.2	–	–
		$Fe_{10}Cr_2B_6$	*C2/m*	33.333	–24.2	–	–
		$Fe_6Cr_2B_4$	*Cmcm*	33.333	–27.5	–	–
		$Fe_2Cr_2B_2$	*Ima2*	33.333	–34.1	–	–
		Cr_2B	*I4/mcm*	33.333	–38.3	–	–

Table 3
Optimized thermodynamic parameters of the binary and ternary systems.

System	Phase	Thermodynamic parameters (J/mol)	Reference
Cr–B	L	${}^{0}L^{L}_{B,Cr} = -175000 + 40.5T$	Present work
		${}^{1}L^{L}_{B,Cr} = -17000$	
		${}^{2}L^{L}_{B.Cr} = 12000$	
	α	${}^{0}L^{\alpha}_{B\,Cr} = -34500$	
	Fe_2B	${}^{\circ}G^{Fe_2B}_{Cr:B} - 0.667\,{}^{\circ}G^{\alpha}_{Cr} - 0.333\,{}^{\circ}G^{(\beta B)}_{B} = -32000 + 7.6T$	
	Cr_2B	${}^{\circ}G^{Cr_2B}_{Cr:B} - 0.667\,{}^{\circ}G^{\alpha}_{Cr} - 0.333\,{}^{\circ}G^{(\beta B)}_{B} = -37550 + 2.53T + 0.1T\ln T + 6\times10^{-4}T^2$	
	Cr_5B_3	${}^{\circ}G^{Cr_5B_3}_{Cr:B} - 0.625\,{}^{\circ}G^{\alpha}_{Cr} - 0.375\,{}^{\circ}G^{(\beta B)}_{B} = -41950 + 0.65T + 0.5T\ln T + 5\times10^{-4}T^2$	
	CrB	${}^{\circ}G^{CrB}_{Cr:B} - 0.5\,{}^{\circ}G^{\alpha}_{Cr} - 0.5\,{}^{\circ}G^{(\beta B)}_{B} = -55000 + 7.8T + 0.1T\ln T + 2\times10^{-4}T^2$	
	FeB	${}^{\circ}G^{FeB}_{Cr:B} - 0.5\,{}^{\circ}G^{\alpha}_{Cr} - 0.5\,{}^{\circ}G^{(\beta B)}_{B} = -28000 + 0.63T$	
	Cr_3B_4	${}^{\circ}G^{Cr_3B_4}_{Cr:B} - 0.4286\,{}^{\circ}G^{\alpha}_{Cr} - 0.5714\,{}^{\circ}G^{(\beta B)}_{B} = -51000 + 2.6T + 0.5T\ln T + 3\times10^{-4}T^2$	
	CrB_2	${}^{\circ}G^{CrB_2}_{Cr:B} - 0.333\,{}^{\circ}G^{\alpha}_{Cr} - 0.667\,{}^{\circ}G^{(\beta B)}_{B} = -36660 + 0.26T + 0.04T\ln T + 3\times10^{-4}T^2$	
		${}^{\circ}G^{CrB_2}_{Va:B} - 0.667\,{}^{\circ}G^{(\beta B)}_{B} = 49554$	
		${}^{\circ}G^{CrB_2}_{Cr:B} - 0.333\,{}^{\circ}G^{\alpha}_{Cr} = 50000$	
		${}^{\circ}G^{CrB_2}_{Va:Va} = 100T$	
	CrB_4	${}^{\circ}G^{CrB_4}_{Cr:B} - 0.2\,{}^{\circ}G^{\alpha}_{Cr} - 0.8\,{}^{\circ}G^{(\beta B)}_{B} = -22620 + 0.207T + 0.108T\ln T$	
Fe–Cr	L	${}^{0}L^{L}_{Cr,Fe} = -14550 + 6.65T$	[26]
	α	${}^{0}L^{\alpha}_{Cr\,Fe} = +20500 - 9.68T$	
		${}^{0}Tc^{\alpha}_{Cr,Fe} = +1650$, ${}^{1}Tc^{\alpha}_{Cr.Fe} = +550$	
		$\beta^{\alpha}_{Cr,Fe} = -0.85$	
	γ	${}^{0}L^{\gamma}_{Cr\,Fe} = +10833 - 7.477T$	
		${}^{1}L^{\gamma}_{Cr,Fe} = 1410$	
	σ	${}^{\circ}G^{\sigma}_{Fe:Cr:Cr} - 0.27\,{}^{\circ}G^{\alpha}_{Fe} - 0.73\,{}^{\circ}G^{\alpha}_{Cr} = +3076 - 3.19T$	
		${}^{\circ}G^{\sigma}_{Fe:Cr:Fe} - 0.27\,{}^{\circ}G^{\gamma}_{Fe} - 0.13\,{}^{\circ}G^{\alpha}_{Cr} - 0.6\,{}^{\circ}G^{\alpha}_{Fe} = 3910 - 3.19T$	
Fe–B	L	${}^{0}L^{L}_{B,Fe} = -140000 + 24.54T$	[3]
		${}^{1}L^{L}_{B,Fe} = 5020$	

		${}^{2}L^{L}_{B,Fe} = 34444$	
	α	${}^{0}L^{\alpha}_{B,Fe} = -79000 + 30T$	
		${}^{0}L^{\alpha}_{B,Fe} = -37000$	
	γ	${}^{0}L^{\gamma}_{B,Fe} = -48000 + 24T$	
		${}^{1}L^{\gamma}_{B,Fe} = -23000$	
	Fe_2B	${}^{\circ}G^{Fe_2B}_{Fe:B} - 0.667\,{}^{\circ}G^{\alpha}_{Fe} - 0.333\,{}^{\circ}G^{(\beta B)}_{B} = -28980 + 2.47T$	
		$Tc^{Fe_2B}_{Fe:B} = 1018,\ \beta^{Fe_2B}_{Fe:B} = 1.91$	
	Cr_2B	${}^{\circ}G^{Cr_2B}_{Fe:B} - 0.667\,{}^{\circ}G^{\alpha}_{Fe} - 0.333\,{}^{\circ}G^{(\beta B)}_{B} = -30000 + 3.2T$	
	Cr_5B_3	${}^{\circ}G^{Cr_5B_3}_{Fe:B} - 0.625\,{}^{\circ}G^{\alpha}_{Fe} - 0.375\,{}^{\circ}G^{(\beta B)}_{B} = 28000$	Present work
	CrB	${}^{\circ}G^{CrB}_{Fe:B} - 0.5\,{}^{\circ}G^{\alpha}_{Fe} - 0.5\,{}^{\circ}G^{(\beta B)}_{B} = -34200 + 22T$	
	FeB	${}^{\circ}G^{FeB}_{Fe:B} - 0.5\,{}^{\circ}G^{\alpha}_{Fe} - 0.5\,{}^{\circ}G^{(\beta B)}_{B} = -36709 + 3.25T$	
		$Tc^{FeB}_{Fe:B} = 600,\ \beta^{FeB}_{Fe:B} = 1.03$	[3]
Fe–Cr–B	L	${}^{0}L^{L}_{B,Cr,Fe} = -70000$	
		${}^{1}L^{L}_{B,Cr,Fe} = -30000$	
		${}^{2}L^{L}_{B,Cr,Fe} = 120000$	
	$(Fe,Cr)_2B$	${}^{0}L^{Cr_2B}_{Cr,Fe:B} = -12000 - 6.5T$	
		${}^{1}L^{Cr_2B}_{Cr,Fe:B} = -62000 + 43T$	
		${}^{2}L^{Cr_2B}_{Cr,Fe:B} = 20000 - 18T$	
	$(Fe,Cr)_2B$	${}^{0}L^{Fe_2B}_{Cr,Fe:B} = -42000 + 12T$	
		${}^{1}L^{Fe_2B}_{Cr,Fe:B} = -94000 + 75T$	Present work
		${}^{2}L^{Fe_2B}_{Cr,Fe:B} = -46500 + 9.15T$	
	Cr_5B_3	${}^{0}L^{Cr_5B_3}_{Cr,Fe:B} = -97000 + 20T$	
		${}^{1}L^{Cr_5B_3}_{Cr,Fe:B} = -30000$	
	(Fe,Cr)B	${}^{0}L^{CrB}_{Cr,Fe:B} = 12000 - 39T$	
		${}^{1}L^{CrB}_{Cr,Fe:B} = -29000 + 23T$	
		${}^{2}L^{CrB}_{Cr,Fe:B} = 25000 - 5T$	
	(Fe,Cr)B	${}^{0}L^{FeB}_{Cr,Fe:B} = -40000 + 7T$	
		${}^{1}L^{FeB}_{Cr,Fe:B} = 5000 - 18T$	

3.1 The Fe–B binary system

The equilibrium phase diagram of the Fe–B binary system is composed of the liquid phase (L), the terminal solutions of Fe (α, γ, and δ) and B (βB), and two intermetallic compounds, Fe_2B (*I4/mcm*) and FeB (*Pbmn*). For this system, we adopted thermodynamic parameters determined by our group /3/, applying the substitutional regular solution model to the solid solutions. The thermodynamic parameters are listed in Table 3, and the calculated Fe–B binary phase diagram is shown in Fig. 1.

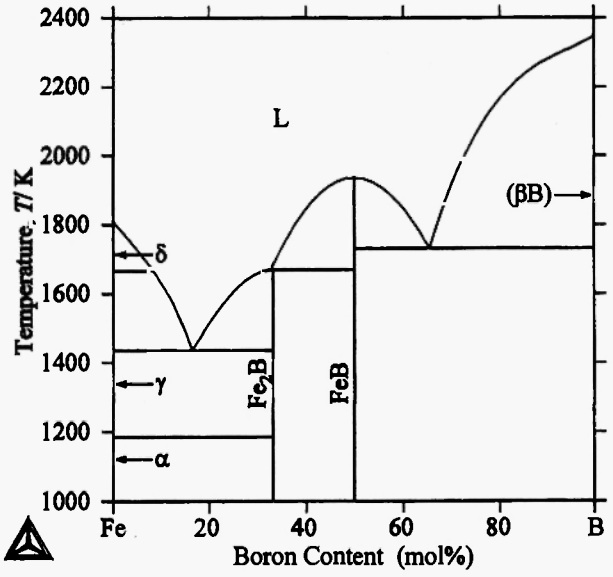

Fig. 1: The calculated Fe–B binary phase diagram.

3.2 The Cr–B binary system

The equilibrium phase diagram of the Cr–B binary system reviewed by Liao and Spear /7/ contains the liquid (L) phase, the terminal solutions of bcc Cr (α) and rhombohedral B (βB), and six intermetallic compounds: Cr_2B (*Fddd*), Cr_5B_3 (*I4/mcm*), CrB (*Cmcm*), Cr_3B_4 (*Immm*), CrB_2 (*P6/mmm*), and CrB_4 (*Immm*). Their assessed phase diagram for the Cr–B system was based on experimental data /8–11/. According to the phase diagram, the solubility of B in α is less than 1.0 mol% B at 1903 K, whereas the maximum solubility of Cr in (βB) is approximately 2 mol%, which is consistent with the experimental results /8,12/. The liquidus and solidus lines were determined by Portnoi *et al.* /8/ using thermal analysis and X-ray diffraction across the range of Cr–B alloys; however, the liquidus temperatures and compositions still remain uncertain.

The solidification in the Cr-rich region occurs by the eutectic reaction as L ⇌ α + Cr_2B at 1902 K. The peritectic reactions as L + Cr_5B_3 ⇌ Cr_2B and L + CrB ⇌ Cr_5B_3 occur at 2143 K and 2173 K, respectively. The congruent melting temperatures of CrB and CrB_2 are reported as 2373 K and 2473 K. The Cr_3B_4 phase forms from the melt by a peritectic reaction with CrB_2 at 2343 K, and the eutectic reaction L ⇌ CrB + Cr_3B_4 takes place at the slightly lower temperature of 2323 K. The B-rich liquid phase solidifies following the eutectic reaction at 2103 K. The CrB_4 phase forms by the peritectoid reaction between the CrB_2 and (βB) at 1773 K. The existence of several other reported phases, such as CrB_6 /13,14/, Cr_4B /14/, β /15/, and MoB-type CrB /16/, are ruled out or still controversial and are not included in the assessed diagram /7/.

The experimental thermodynamic data for the Cr–B system are very limited. The enthalpy of formation of CrB_2 varies, ranging from –31.3 to –39.7 kJ/mol of CrB_2 /17–19/. The heat capacity values for borides have been measured in several studies. The high-temperature heat capacities of CrB and CrB_2 were measured experimentally by Krestovnikov and Vendrikh /20/ and Mezaki *et al.* /21/. Hack and Chart /22/ estimated the heat capacities for the borides from these experimental values, considering the trends shown by values for Co, Fe, Mo, Ti, and W borides.

Thermodynamic assessment of the Cr–B binary system was carried out by Campbell and Kattner /23/, treating B as an interstitial element in the fcc and bcc solid solution phases. Hack and Chart /22/ also calculated the Cr–B phase diagram. The atomic diameter of B is 1.8 Å, which is too small to occupy a substitutional position in Fe and too large to locate in the octahedral interstitial sites in ferrite or austenite. We analyzed the behavior of B in solid solutions in the Fe–B binary system using a first-principles method /3/. The results revealed that, at least in the ground state, B atoms substitute for the Fe atoms in the solid solutions. Furthermore, presumably because of inadequacy of the formation energies of borides, the thermodynamic parameters of this binary system were found by

Campbell and Kattner /23/ to cause instability of the CrB phase at temperatures below 1273 K, making the reproduction of an experimental phase boundary of the Fe–Cr–B ternary system more difficult. Thus, the thermodynamic analysis of this binary system was performed based on the above-mentioned experimental information on the phase boundaries and invariant reactions, as well as the calculated enthalpy of formation for the three types of Cr borides, using first-principles calculations. Information on the crystallographic data was obtained from the compilation by Villars /24/. The evaluated heat capacities of borides /22/ were also considered to estimate the temperature dependence of the formation energy for these compound phases.

The enthalpies of formation of the Cr-borides are compared with experimental work and the previous assessment /23/ in Table 2. The listed values denote the enthalpy of formation based on bcc Cr, and rhombohedral αB with the *hR*12-type structure. The calculated enthalpy of formation of CrB_2 has been determined to be –33.3 kJ/mol, which agrees well with the experimental value measured by Topor and Kleppa /19/. However, the value for the enthalpy of formation of the CrB phase (–37.8 kJ/mol) by the previous assessment /23/ was found to be too small to be stable at lower temperature.

The optimized thermodynamic parameters are listed in Table 3. The calculated values for the heat capacity of the Cr_2B and Cr_5B_3 phases were compared with the evaluated values /22/ in Fig. 2 (a) and (b), respectively. Figure 3 shows a comparison of the calculated and invariant reactions data of the Cr–B binary phase diagram. It can be seen from these figures that the evaluated parameters show a good agreement with the corresponding experimental data on the phase boundaries.

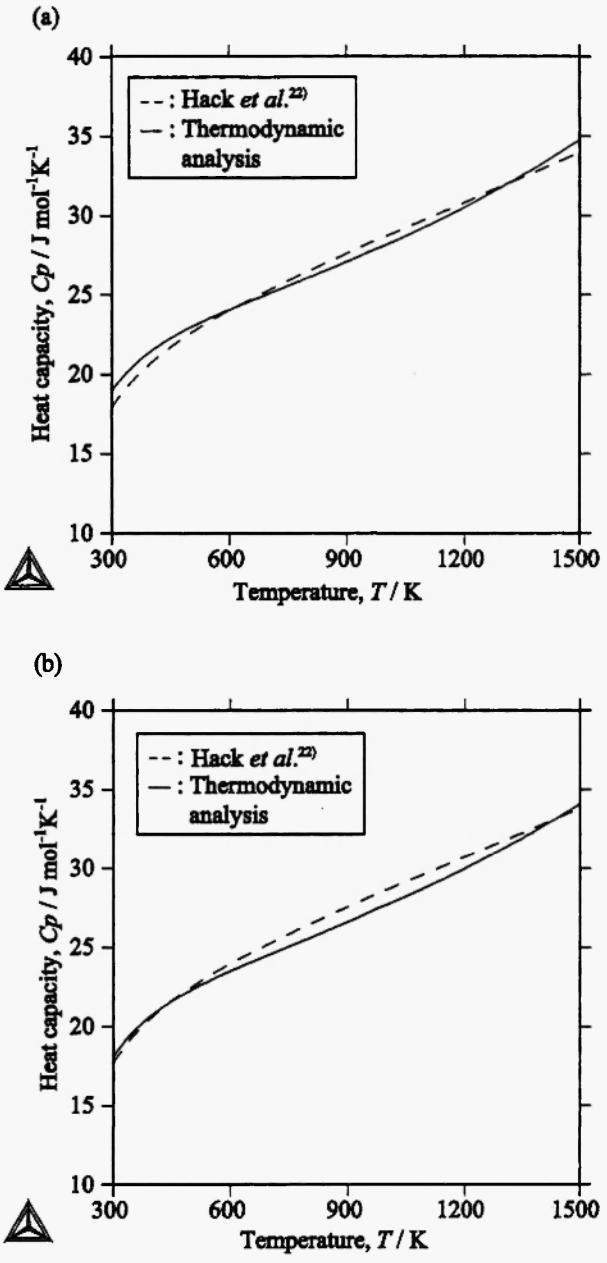

Fig. 2: (a) Heat capacity versus temperature diagram for Cr_2B. (b) Heat capacity versus temperature diagram for Cr_5B_3.

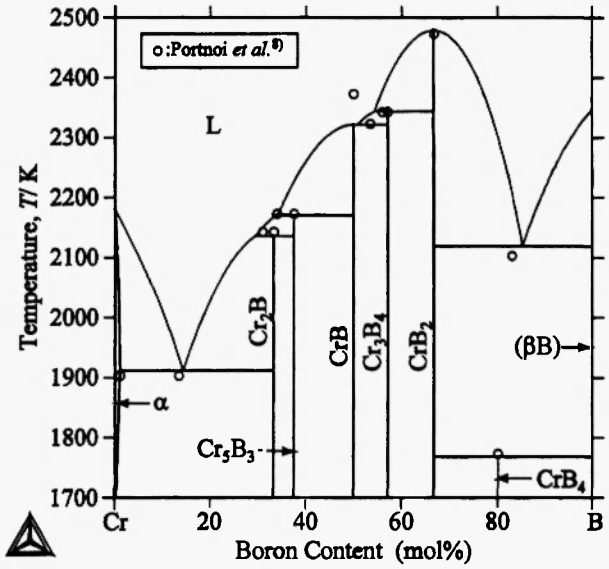

Fig. 3: The calculated Cr–B binary phase diagram compared with the experimental phase boundaries.3.3 The Fe–Cr binary system

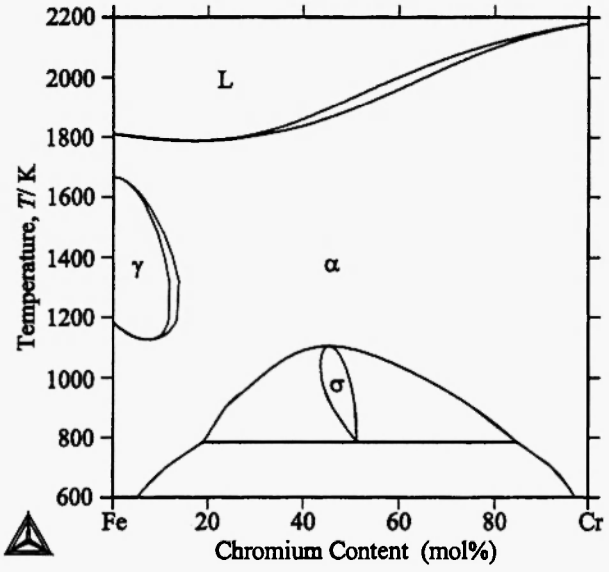

Fig. 4: The calculated Fe–Cr binary phase diagram.

The equilibrium phases in the Fe–Cr binary system are the liquid (L) phase, the bcc continuous solid solution (α and δ), the terminal fcc solid solution (γ), and the intermediate σ phase, which is formed at 1093 K and decomposes by eutectoid reaction with the separated bcc solutions below 813 K /25/. The thermodynamic calculation was performed many times based on the different thermodynamic models, and we accepted the parameters of Andersson and Sundman /26/, considering the consistency of the thermodynamic models with the present work. The calculated Fe–Cr binary phase diagram is shown in Fig. 4.

3.4 The Fe–Cr–B ternary system

The isothermal section of the ternary system is composed of the Fe_2B, FeB, Cr_2B, Cr_5B_3, CrB, Cr_3B_4, CrB_2, and CrB_4 phases in addition to liquid and terminal solid solutions, and no ternary compound has been reported. As mentioned in the previous section, some indeterminate binary borides, such as CrB_6 or Cr_4B, which appear in an experimental phase diagram /14/, were excluded from the present assessment.

Concerning the Fe–Cr–B ternary system, there is some experimental information on phase equilibria determined at 973 and 1173 K /13/ and at 1373 K /14/ across the entire ternary system. The isothermal sections of the Fe–Cr–B ternary system with a B content up to 50 mol% were also studied at the temperatures of 1373 K /27/ and 1523 K /15/, using metallographic and X-ray diffraction methods. Compared with other experimental data, the isothermal section diagram at 1373 K given by Gorbunov and Boduryan /14/ shows that the α phase equilibrium with the Fe_2B phase and the Cr_2B phase extends considerably toward the Cr-rich side. Thus, concerning the phase equilibria at 1373 K, the reported values by Gianoglio /27/ could be more reliable. Shirae *et al.* /16/ investigated the phase diagram of the pseudo-binary FeB–CrB section in the temperature range from 1173 to 2473 K using the high-temperature X-ray diffractometer and vibrating sample magnetometer.

Among the binary borides, the solubilities of Fe in Cr_3B_4, CrB_2, and CrB_4 are very small and negligible. However, about 24 and 50 mol% of Fe atoms in the Fe_2B and FeB phases, respectively, could be substituted with Cr atoms /13,27/. Gianoglio *et al.* /27/ also examined the phase relationship of coexistence between the Cr borides and concluded that the solubilities of Fe in the Cr_2B, Cr_5B_3 and CrB phases possibly reach up to 65, 12 and 30 mol%, respectively.

There is no experimental information available on the thermodynamic properties of this ternary system, and we attempted to evaluate variations of the formation enthalpies for the Fe_2B (*I4/mcm*) and CrB (*Cmcm*) with

dissolving Cr and Fe, respectively, using first-principles calculations. Superstructures for computing the formation energies were constructed by changing the stack of atoms along a given direction of the parent lattice structures /3,28,29/. The calculated results are summarized in Table 2 with the space group of the constructed superstructures.

Thermodynamic analysis of the present study was performed using the experimental isothermal section diagrams at 973 K, 1173 K /13/ and 1373 K /27/, the phase boundaries of the pseudobinary FeB–CrB section /16/, and the enthalpies of formation along the lines of Fe_2B–Cr_2B (*I4/mcm*) and FeB–CrB (*Cmcm*) sections determined using the first-principles calculations. The experimental basal projection of liquidus surfaces /30/ was also taken into account to estimate the ternary interaction parameters affected in the Fe-rich melt. The optimized thermodynamic parameters are summarized in Table 3. The calculated enthalpies of formation of the FeB–CrB and Fe_2B–Cr_2B pseudobinary sections were shown in Fig. 5 (a) and (b), where the solid lines represent the results obtained by the thermodynamic analysis. In the ground state, these borides show phase separation. The calculated isothermal sections at 973 K, 1173 K, and 1373 K are shown in Fig. 6 (a)–(c), in comparison with the experimental results /13,27/. In general, the calculated phase boundaries correspond well with the experimental fields, although locations of some narrow three-phase fields such as $\gamma + Fe_2B + Cr_2B$ at 1373 K show slight deviation from the experimental data. In Figure 7, the calculated phase diagram of the pseudobinary FeB–CrB system is compared with the experimental phase fields /16/. The agreement seems fairly good, except for the lower temperature range below around 1273 K. However, Shirae *et al.* /16/ noted that a two-phase mixture of (FeB + CrB) below 1393 K changed irreversibly to a single phase with the CrB phase, and it was not obvious whether two-phase mixing at a temperature below 1393 K is an equilibrium state. Thus, it might that further discussion of this point would be irrelevant. The calculated whole range of liquidus projection of this ternary system presented in Fig. 8 (a) can be compared with the experimental phase diagram /30/ in Fig. 8 (b).

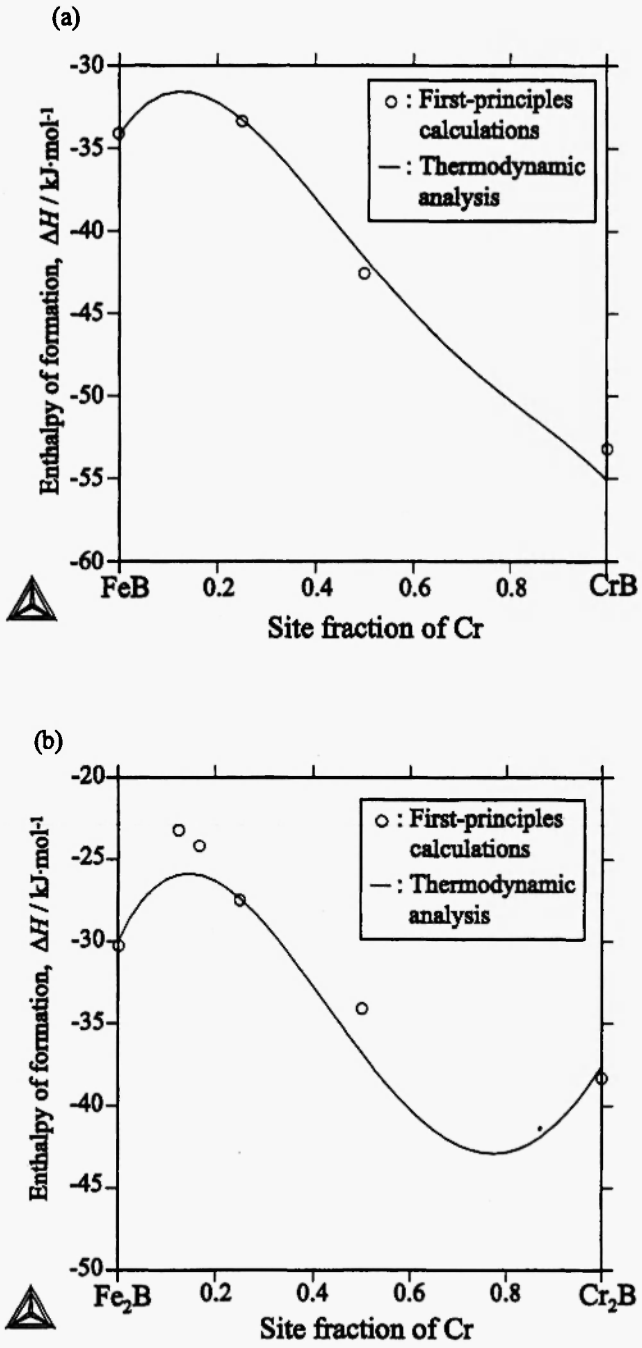

Fig. 5: The calculated enthalpy of formation for (a) FeB–CrB, and (b) Fe_2B–Cr_2B pseudobinary sections in the Fe–Cr–B ternary system.

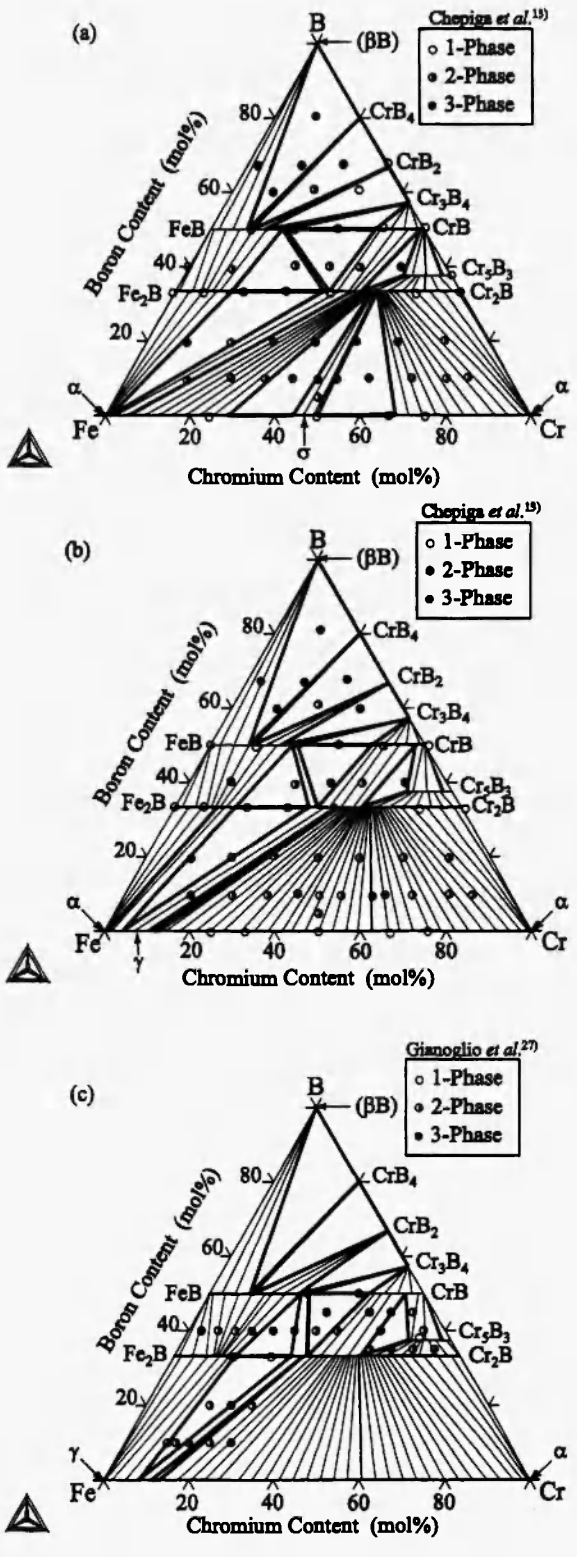

Fig. 6: A calculated isothermal section diagram of the Fe–Cr–B system at (a) 973 K, (b) 1173 K, and (c) 1373 K.

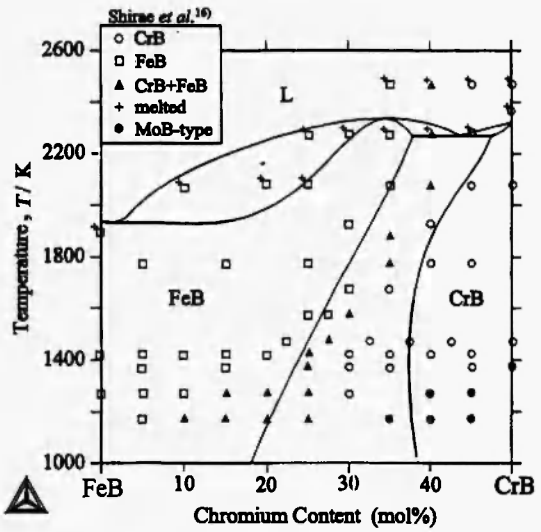

Fig. 7: The calculated vertical section diagram of the Fe–Cr–B system.

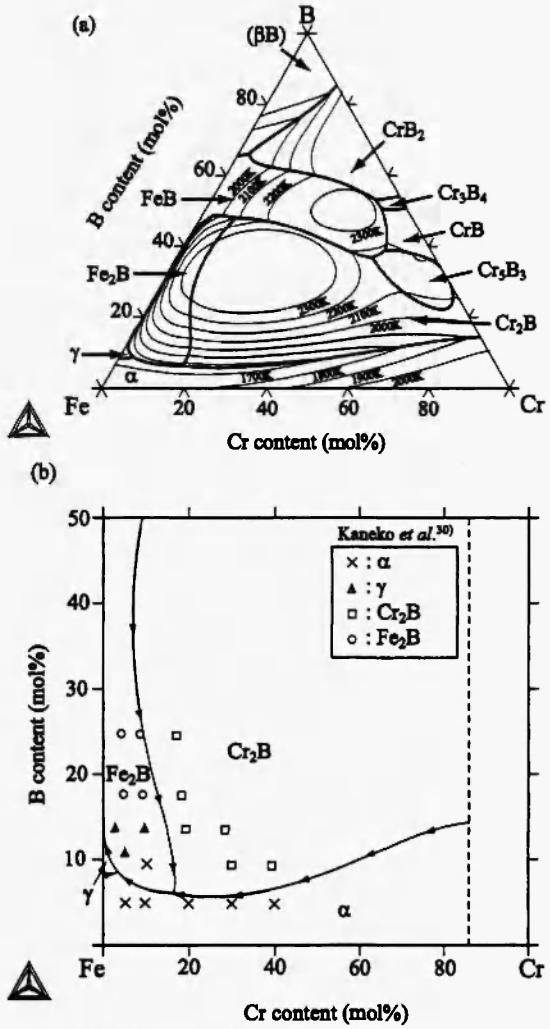

Fig. 8: (a) The calculated liquidus projection of the Fe–Cr–B system, and (b) Fe-rich side.

4. CONCLUSIONS

A thermodynamic analysis of the Fe–Cr–B ternary system was performed, applying the substitutional-type regular solution model to the solid solutions. For the Fe–B and Fe–Cr binary systems, thermodynamic parameters evaluated by the previous analysis were used in the present study, and the following results were obtained.

1. The thermodynamic analysis of the Cr–B binary system was carried out based on experimental information concerning phase boundaries and heat capacity data, as well as the calculated enthalpies of formation for the Cr_2B, Cr_5B_3, CrB, Cr_3B_4, CrB_2, and CrB_4 phases, using first-principles calculations. The calculated enthalpy of formation of CrB_2 agrees well with the experimental value. However, first-principles calculations revealed that the previous thermodynamic assessment for the absolute value of the enthalpy of formation of the CrB phase was too small to be stable at low temperature. The evaluated parameters show a good agreement with the corresponding invariant reactions data of the Cr–B binary phase diagram.
2. Because of a lack of experimental information on the thermodynamic properties of the ternary system, variations of the formation enthalpies for the Fe_2B (*I4/mcm*) and CrB (*Cmcm*) with dissolving Cr and Fe were evaluated using first-principles calculations. The phase equilibria of the Fe–Cr–B ternary system were elucidated across the entire composition range by determining the thermodynamic functions based on the theoretical values and on any available experimental information.

ACKNOWLEDGMENTS

The authors gratefully acknowledge financial support from the Nippon Steel Co. Ltd. for this work.

REFERENCES

1. P. Blaha, K. Schwarz, G. K. H. Madsen, D. Kvasnicka, J. Luiz, *WIEN2k, An Augmented Plane Wave and Local Orbitals Program for Calculating Crystal Properties* (Karlheinz Schwarz, Technische Universität Wien, Austria) 2001. ISBN 3-9501031-1-2.
2. J. P. Perdew, K. Burke, Y. Wang, *Phys. Rev.* **B 54**, 16533–16539 (1996).
3. K. Yoshitomi, Y. Nakama, H. Ohtani, M. Hasebe, *ISIJ Int.* **48**, 835–844 (2008).
4. G. Inden, Proc. Calphad V, Max-Planck Inst. Eisenforsh. G.m.b.H, Düsseldorf, *III*-(4)-1 (1976).
5. M. Hillert, M. Jarl, *Calphad*, **2**, 227–238 (1978).
6. A.T. Dinsdale, *Calphad*, **15**, 317–425 (1991).
7. P.K. Liao and K.E. Spear, *Phase Diagram of Binary Iron Alloys*, ASM, Metals Park, Ohio, USA, 41–47 (1993).
8. K.I. Portnoi, V.M. Romashov and I. V. Romanovich, *Poroshk. Metall.*, 4(76), 51–57 (1969).
9. K.I. Portnoi and V.M. Romashov, *Poroshk. Metall.*, **5(113)**, 48–56 (1972).
10. C.N. Guy and A.A Uraz, *J. Less-Common Met.*, **48**, 199–203 (1976).
11. S. Andersson and T. Lundstrom, *Acta Chem. Scand.*, **22**, 3101–3110 (1968).
12. S. Andersson and T. Lundstrom, *J. Solid State Chem.*, **2**, 603–611 (1970).
13. M.V. Chepiga and Yu.B. Kuz'ma, *Chernaya Met.* **3**, 127–130 (1970).
14. A.E. Gorbunov and F.N. Boduryan, *Met. Tverd. Splavov*, **16**, 172–178 (1976).
15. M. Lucco Bprlera and G. Pradelli, *Met. Ital.*, **65**, 421–424 (1973).
16. K. Shirae, Y. Ueda, S. Kachi, and K. Kosuge, *Mat. Res. Bull.*, **22**, 521–526 (1987).
17. O. Kubaschewski and C.B. Alcock, *Metallurgical Thermochemistry*, 5th ed., Pergamon Press, New York (1979).

18. A.K. Niessen and F.R. DeBoer, *J. Less-Common Met.*, **82**, 75–80 (1981).
19. L. Topor and O.J. Kleppa, *J. Chem. Thermodyn.*, **17(2)**, 109–116 (1985).
20. A.N. Krestovnikov and M.S. Vendrikh, *Sb. Nauchn. Tr. Inst. Tsvetn. Metall.*, **33**, 3–7 (1960).
21. R. Mezaki, E.W. Tilleux, D.W. Barnes, and J.L. Margrave, *Thermodynamics of Nuclear Materials*, IAEA, Vienna (1962)
22. K. Hack and T.G. Chart, Div. Mater. Appl., Natl. Phys. Lab., Teddington, UK, Comm. Eur. Communities, EUR7820, Pt.2 (1982).
23. C.E. Campbell and U.R. Kattner, *Calphad*, **26**, 477–490 (2002).
24. P. Villars, *Pearson's Handbook, Desk Edition, Crystallographic Data for Intermetallic Phases, Vol.1*, ASM International, Materials Park, Ohio, USA (1997).
25. V.P. Itkin, *Phase Diagrams of Binary Iron Alloys*, ASM International, Materials Park, Ohio, USA, 102–129 (1993).
26. J.-O. Andersson and B. Sundman, *Calphad*, **11**, 83–92 (1987).
27. C. Gianoglio, G. Pradelli and M. Vallino, *Metallurgical Science and Technology*, **1**, 51–57 (1983).
28. Z. W. Lu, S.-H. Wei, A. Zunger, S. Frota-Pessoa, L. G. Ferreira, *Phys. Rev.* **B 44**, 512–544 (1991).
29. A. van de Walle, G. Ceder, *J. Phase Equil.* **23**, 348–359 (2002).
30. H. Kaneko, T. Nishizawa and A. Chiba, *J. Jpn. Inst. Met.*, **30**, 157–163 (1966).
31. O.S. Gorelkin, A.S. Dubrovin, O.D. Kolesnikova and N.A. Chirkov, *Russ. J. Phys. Chem.*, **46**, 431–432 (1972).
32. S. Omori and J. Moriyama, *Trans. Jpn. Inst. Met.*, **21**, 790–796 (1980).
33. S. Sato and O.J. Kleppa, *Metall. Trans.*, B, **13B**, 251–257 (1982).